IEEE Access
Multidisciplinary | Rapid Review | Open Access Journal

Received June 26, 2019, accepted August 2, 2019, date of publication August 6, 2019, date of current version September 4, 2019.

Digital Object Identifier 10.1109/ACCESS.2019.2933450

Numerical Study on the Prediction of "Sweet Spots" in a Low Efficiency-Tight Gas Sandstone Reservoir Based on a 3D Strain Energy Model

SHUAI YIN[1,2,3] AND ZHIYOU GAO[4]

[1]School of Earth Science and Engineering, Xi'an Shiyou University, Xi'an 710065, China
[2]State Key Laboratory of Oil and Gas Reservoir Geology and Exploitation, Chengdu University of Technology, Chengdu 610059, China
[3]Shanxi Key Laboratory of Petroleum Accumulation Geology, School of Earth Science and Engineering, Xi'an Shiyou University, Xi'an 710065, China
[4]Shandong Geo-Mineral Engineering Group Company Ltd., Jinan 250200, China

Corresponding author: Shuai Yin (speedysys@163.com)

This work was supported by the Open Fund of the State Key Laboratory of Oil and Gas Reservoir Geology and Exploitation, Chengdu University of Technology, under Grant PLC20190205.

ABSTRACT The study of the construction of a micro-scale rupture parameter from the perspective of rock stress and strain is a frontier in geoscience. The strain energy density (U) can quantitatively characterize the probability of internal micro-scale ruptures in different types of rock. Based on this, in this paper, a systematic forecasting method for tight sandstone sweet spots in a low-amplitude tectonic zone based on U-value calculations was proposed. The specific steps are as follows. First, a geological model of the target layer was created, and a new rock mechanics parameter assignment method based on sedimentary facies control principle was proposed. Then, the palaeo-tectonic stress field of the target layer in the Yanshanian period was recovered through the boundary loading. Finally, the strain energy density distribution of the target layer was obtained based on energy conservation principle. The simulation results of the paleo-tectonic stress field show that, the distribution of horizontal stress is mainly affected by lithology and local structure, and the vertical stress is mainly affected by the burial depth. Stress diffusion occurs in some areas, which are mainly affected by lithologic mutations or complex structures. The U values of the target layers have a band-like distribution and are mainly distributed between 0.12 and 0.30 J·m^{-3}. The relationship between strain energy density and productivity of tight sandstone reservoirs was analyzed, and the criteria for distinguishing sweet spot areas based on U values were proposed. This method is applicable to strongly heterogeneous tight sandstone reservoirs in the low-amplitude tectonic zone of the Ordos Basin and have reference values for similar types of reservoirs around the world.

INDEX TERMS Tight gas sandstone, strain energy model, finite element method, tectonic stress field.

I. INTRODUCTION

The Ordos Basin is located in the western region of the North China tectonic plate. It is a multi-cycle superimposed basin formed by the transformation of multiple Paleozoic and Mesozoic sedimentary basins [1]–[7]. The Ordos Basin is an important energy production base in China [8]–[11]. Its natural gas resources are mainly distributed in the tight sandstone of the Upper Paleozoic strata [12], [13]. The Permian He8 member in the basin is an important production layer of the Upper Paleozoic sedimentary system. The widely distributed natural gas in this reservoir has large gas-bearing degree differences [14]. For the sandstone reservoir in the Permian He8 member, the daily gas production per well is generally less than 1×10^4 m^3, which makes it a typical low efficiency reservoir.

To explore the regularity of natural gas enrichment in the He8 reservoir, the previous researchers have conducted extensive investigations on the reservoir characteristics, diagenesis, and reservoir sedimentation [15]–[17]. The characteristics of gas accumulation in the He8 reservoir are mainly affected by the microscopic pore structure. The pore types of the He8 reservoirs include residual primary intergranular pores, intergranular dissolution pores,

The associate editor coordinating the review of this article and approving it for publication was Trivikram Rao Molugu.

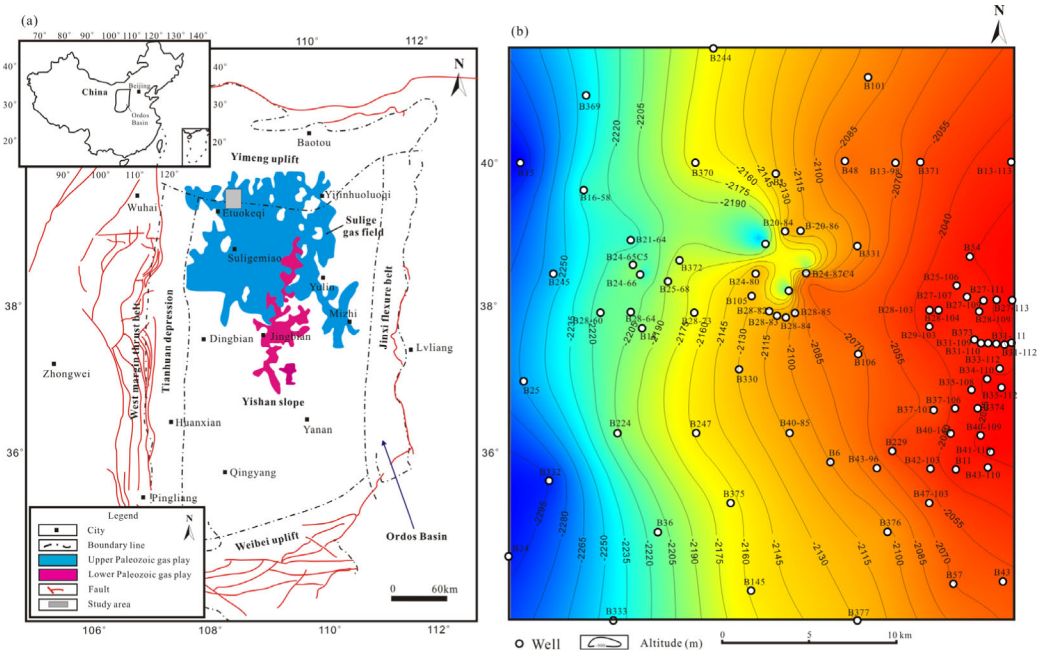

FIGURE 1. (a) The study area is located in the northwestern part of the Sulige gas field in the Ordos Basin; (b) Contour map of the study area in the bottom of the Permian Lower Shihezi Formation.

intragranular dissolution pores, intercrystalline pores, and microfractures [18], [19]. The microfractures include interparticle microfractures, particle-penetrated microfractures, and network microfractures [18], [20]–[23]. The existence of a large number of microfractures effectively enhances the connectivity of different types of pores and is an important factor in the formation of tight sandstone sweet spots [24]–[26].

Microfractures represent the lowest level of rupture order [27]–[31]. At present, research on microfractures in tight reservoirs is mainly focused on experimental tests and microscopic observations. Research on the planar distribution prediction methods of microfractures is still very limited [7], [32]–[37]. Rock rupture characteristics are mainly controlled by rock mechanics properties and the stress environment [2], [10], [38], [39]. Therefore, by recovering the paleo-tectonic stress field during the formation period of fractures, and combining certain rupture criteria, an effective prediction of the micro-scale rupture zones can be achieved [40]–[42].

In the past, the rock mechanics parameters were generally assigned using the structural divisions or a simple Kriging interpolation method [43]. The structural division assignment is to divide the target layer into several types of structural areas, such as folds, faults and gentle belts, and then assign values to the rock mechanics parameters of different structural areas. The Kriging interpolation method predicts the distribution of plane rock mechanics parameters based on the logging interpretation results of single well rock mechanics parameters and the Kriging interpolation calculations [44]. Obviously, neither of these methods considers the influence of sand body spreading on rock mechanics parameters. In order to overcome this deficiency, in this paper, a new rock mechanics parameter assignment method based on sedimentary facies control principle was proposed to assign rock mechanics parameters. This method can more directly reflect the control effect of river sediments on rock mechanics parameters.

Strain energy density (U) can quantitatively characterize the distribution of strain energy in different types of rock. When the energy exceeds the rock particles' strength limit, the rock will produce micro-scale ruptures [45]–[48]. This parameter is extremely effective in predicting the probability of microscale ruptures of rock mass. Therefore, the relationship between strain energy density and single well productivity was discussed in this paper, and the reservoir sweet spots were predicted. This study has reference value for the exploration of similar tight gas sandstone reservoirs worldwide.

II. GEOLOGICAL SETTING

A. STRUCTURAL FEATURES

The tectonic units of the Ordos Basin include the Tianhuan Depression, the Jinxi Flexural Belt, the Weibei Uplift, the Yimeng Uplift, the Yishan Slope and the West Margin Thrust Belt (Fig. 1a). The study area is located in the northwestern region of the Sulige gas field, which is between the Yishan Slope and the Yimeng Uplift (Fig. 1a). The stratum of the study area is relatively flat, and the degree of structural deformation is low, and some low-amplitude tectonics are developed [49], [50]. According to the contour map of the bottom of the Permian He8 member (Fig. 1b), the structure of the study area is a broad, westwardly inclined, regionally

Strata				Sedimentary facies	
System	Series	Formation	Segment	Microfacies	Subfacies
Permian	Upper	Shiqianfeng Formation	Qian1	Underwater distributary channel, channel bay	Braided river delta plain
			Qian2		
			Qian3		
			Qian4		
			Qian5		
	Middle	Upper Shihezi Formation	He1	Distributary channel, channel bay	Meandering river delta plain
			He2		
			He3	River channel, river flood plain	
			He4		
		Lower Shihezi Formation	He5	Distributary channel, channel bay	Braided river delta plain
			He6		
			He7		
			He8		
	Lower	Shanxi Formation	Shan1	River channel, river flood swamp	Meandering river delta plain
			Shan2		
		Taiyuan Formation	Tai1	Sand flat, limestone flat, peat flat	Tidal flat
			Tai2		
Carbonife-rous	Upper	Benxi Formation	Ben1		
			Ben2		

FIGURE 2. Depositional unit division of the study area. The target layer is located in the Permian He8 member, with a depth of approximately 3 400 to 3 800 m and a thickness of approximately 50 to 80 m. The He8 reservoir is a braided river sedimentary system.

large monocline. Low-amplitude nose-like structures are distributed over the wide, gentle slope. There are no faults in the study area, indicating that the tectonic activities were weak [6].

B. DEPOSITIONAL UNIT AND RESERVOIR

The sedimentary stratigraphic units in the study area are shown in Fig. 2. The main gas producing layer in the Upper Paleozoic strata is located in the Permian He8 member, with a depth of approximately 3 400 to 3 800 m and a thickness of approximately 50 to 80 m. The He8 reservoir is a braided river sedimentary system. The lithology of the sandstone reservoirs is characterized by coarse granularity and large variations, including lithic quartz sandstones and quartz sandstones. The sandstones have a porosity of 5%-12% and a permeability of $0.01 - 2 \times 10^{-3}$ μm^2, which is typical of a low-porosity and low-permeability tight sandstone reservoir [51].

Microfractures in the He8 target layer are well developed, and these microfractures generally have good directionality (Fig. 3). These microfractures can be divided into large-opening fractures and small-opening fractures from the opening and extension length (Fig. 3a). Fig. 3b shows the fluorescent characteristics of the microfractures and inclusions in the He8 tight sandstone reservoir of the Sulige gas field [18]. The uniform temperature test results showed that these microfractures were formed in the Yanshanian period [18]. These microfractures are generally distributed inside the particles or cut through the particles being affected by the compressive stress [29], [52]. The inclusions appear beaded and distributed along the microfractures (Fig. 3b). For the superficial F_1 microfractures without cutting through the particle, the inclusions were essentially non-fluorescent, representing early brine inclusions without hydrocarbons; for the superficial F_2 and F_3 microfractures cutting through the particle, the brine inclusions containing hydrocarbons show significant fluorescence, indicating that they were formed in another stage (Fig. 3b) [18]. The microfractures of the He8 tight sandstone are generally distributed at the edge and inside of the quartz particles (Fig. 3c-d). Microfractures are related to the migration of hydrocarbons and the formation of reservoirs.

III. PALAEO-TECTONIC STRESS FIELD SIMULATION

The calculation of the strain energy density is based on the recovery of the tectonic stress field [47], [53]. Therefore, 3D FEM (Finite Element Method) technology was used to recover the paleo-tectonic stress field of the target layer first. The 3D FEM method is a commonly used method for tectonic stress field simulation [54]. The plane distribution of the stress is obtained by the mechanical unit assignments and boundary constraints [55].

A. MODEL BUILDING AND UNIT DIVISION

ANSYS software was used to perform the 3D FEM modeling and analysis. The modeling process was based on principal of point to line to surface [48]. We used the structural data of the target layer (He8 member) to creat the 3D geological model [48]. First, the spline curves were generated using ANSYS command flows, then, the curved surface will be generated. Finally, the 3D model of the target layer was generated based on the trend surface analysis theory [56]–[58].

TABLE 1. Unit type and quantity in the finite element model.

Strata	Number of units	
	Nodes	Elements
Upper He8-1 member	156 283	643 275
Upper He8-2 member	149 655	537 298
Lower He8-1 member	163 279	643 369
Lower He8-2 member	158 473	663 583

The 3D FEM model of the He8 member was divided into 4 layers (Fig. 4), including the Upper He8-1 and He8-2 members, Lower He8-1 and He8-2 members, respectively. Then, the established model was divided into a series of grid cells, including tetrahedrons, pentahedrons and hexahedrons. The unit types and quantities of the 4 layers are shown in Table 1. In complex structure sites, the mesh density was increased, which increases the computation but improves the planar resolution of the calculation results. The grid has an accuracy of 20 m.

B. ASSIGNMENT OF ROCK MECHANICS PARAMETERS

The sedimentary facies of the He8 member sandstone is determined according to the sandstone ratio (SMR). The ratio of cumulative sandstone thickness to total formation thickness

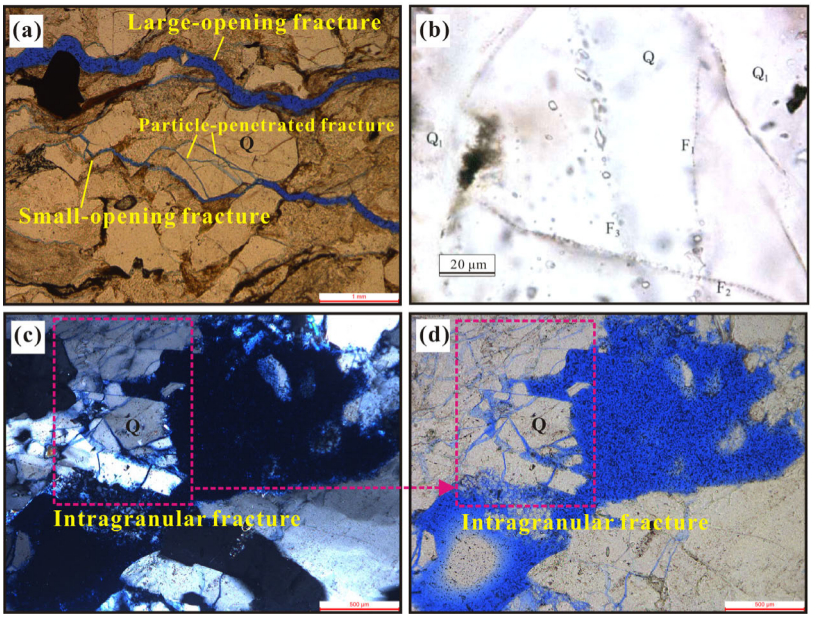

FIGURE 3. Fluorescent characteristics of microfractures and inclusions in the He8 tight sandstone reservoir in the Sulige gas field. Notes: (a) Well B373, 3 435.6 m, collected from a gas layer, Q—Quartz particle; (b) Samples were collected from the Wushenzhao area in the northern part of the Sulige gas field [18]. Q_1—Authentic quartz overgrowth; F_1, F_2 and F_3—Microfractures on the surface of the quartz particle, F_1 did not cut through the quartz particle, F_2 and F_3 cut through the quartz particle; (c-d) Well 139, 3 640.61 m, cracked quartz particles, collected from a gas layer. c—Orthogonal polarized image, d—single polarized image.

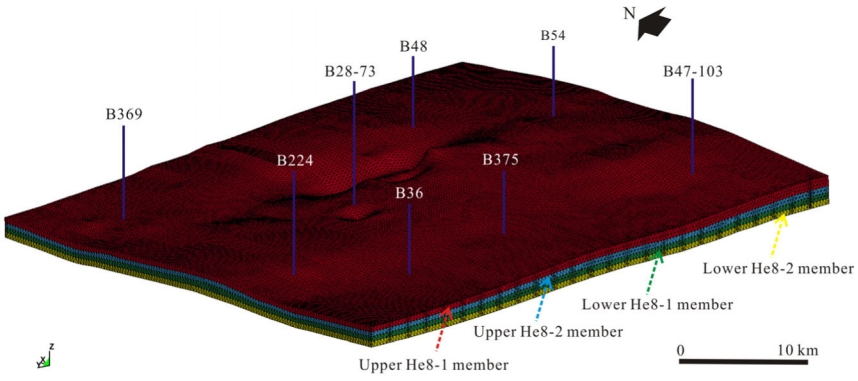

FIGURE 4. 3D finite element model of the He8 member in the study area.

is SMR [59]. The sedimentary facies of the He8 member include a distributary bay (SMR<20%) (Fig. 5a-c) and a distributary channel (SMR≥20%) (Fig. 5d) [60].

According to the logging interpretation results of rock mechanics parameters that have been statically corrected. We compared the relationship between SMR and rock mechanics parameters. It can be found that there is a strong positive correlation between SMR and Young's modulus (E) (Eq. 1, the correlation coefficient=0.891), while there is a strong negative correlation between SMR and Poisson's ratio (ν) (Eq. 2, the correlation coefficient=0.778). Then, the Young's modulus and Poisson's ratio were assigned based on the SMR. The study production layer is located in the Lower He8 member, and the distribution of the Young's modulus and the Poisson's ratio of the two sub-layers are shown in Fig. 6.

$$E = 0.158 \cdot \mathrm{SMR} + 21.37 \quad (1)$$

$$\nu = -0.0005 \cdot \mathrm{SMR} + 0.275 \quad (2)$$

where SMR is the sandstone ratio; E is Young's modulus, GPa; and ν is Poisson's ratio.

From Fig. 6, it can be seen that the high Young's modulus value areas corresponds to the low Poisson's ratio value areas. E of the target layer is ranging from 22 to 35 GPa, and ν is ranging from 0.24 to 0.27.

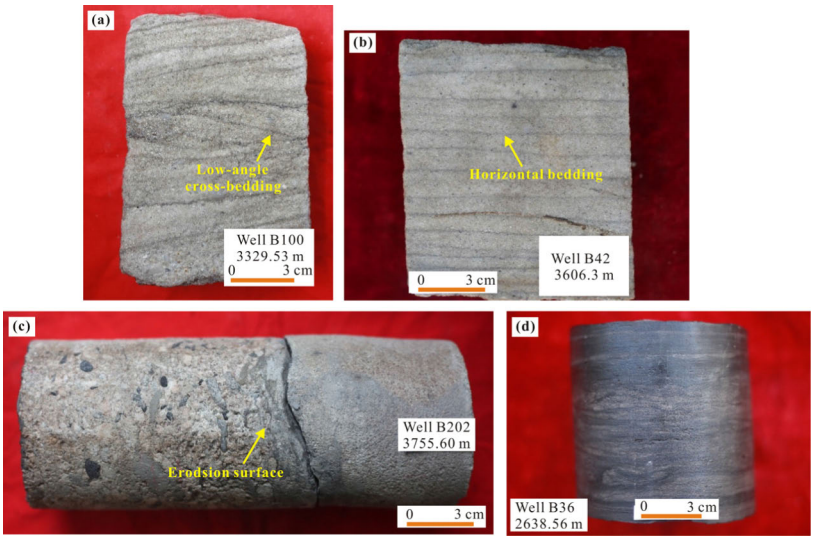

FIGURE 5. Core characteristics in the He8 member. Notes: (a) Well B100, 3 329.53 m, sandstone, low angle cross-bedding, distributary channel sendiments; (b) Well B42, 3 606.3 m, medium-fine sandstone interbeded with horizontal shale laminae, distributary channel sendiments; (c) Well B202, 3 755.6 m, gravel-bearing medium- coarse sandstone, bottom of distributary channel sendiments; (d) Well B36, 2 638.56 m, black mudstone interbeded with thin fine sandstone, distributary bay sendiments.

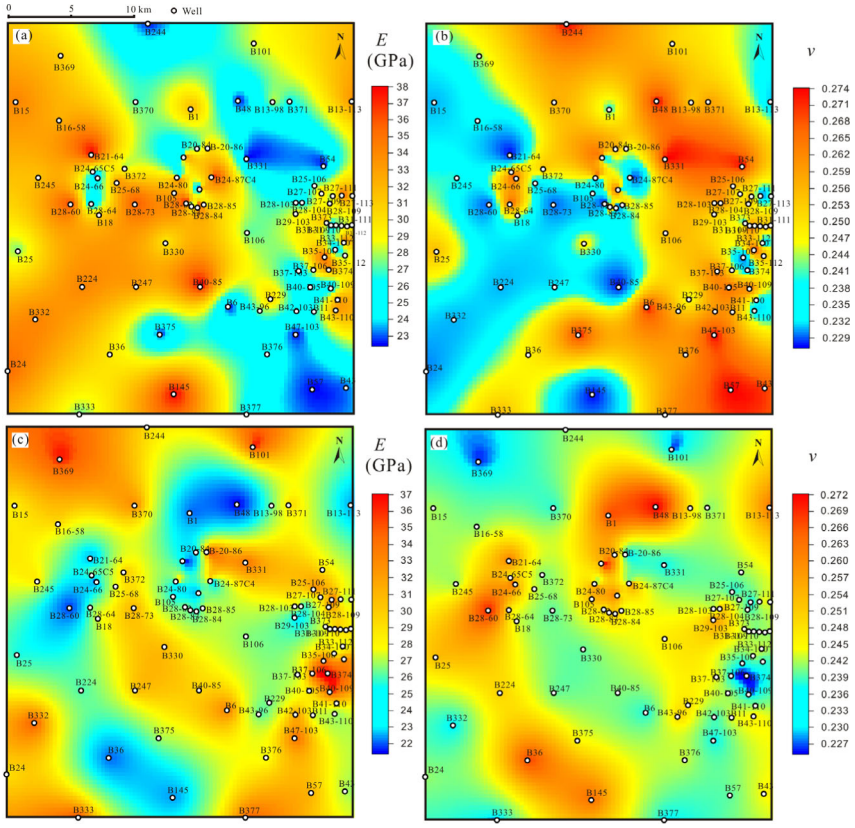

FIGURE 6. Planar distribution of Young's modulus and Poisson's ratio of the target layer. Notes: (a) Young's modulus, Lower He8-1 member; (b) Poisson's ratio, Lower He8-1 member; (c) Young's modulus, Lower He8-2 member; (b) Poisson's ratio, Lower He8-2 member.

For the other parameters, such as rock density (ρ), cohesion (C) and internal friction angle (φ), their magnitude does not have significant difference. Therefore, the assignment of these parameters is shown in Table 2. This assignment method is also based on the sedimentary facies control principle, and it is applicable to tight reservoirs [61].

TABLE 2. Assignment results of rock mechanics parameters.

Formation	Sedimentary facies	SMR	ρ ($g \cdot cm^{-3}$)	C (MPa)	φ (°)
He8 member	Distributary bay	SMR<20%	2.52	10.58	37.13
	Distributary channel	20%≤SMR<40%	2.55	14.26	40.26
	Distributary channel	40%≤SMR<60%	2.58	15.13	40.68
	Distributary channel	60%≤SMR<80%	2.59	15.27	42.46
	Distributary channel	SMR≥80%	2.58	17.45	42.83

Using the sedimentary facies control principle to assign rock mechanics parameters is consistent with the sedimentary characteristics of sand bodies and the objective distribution law of rock mechanics parameters. Thus this method can ensure the reliability of the tectonic stress field simulation results.

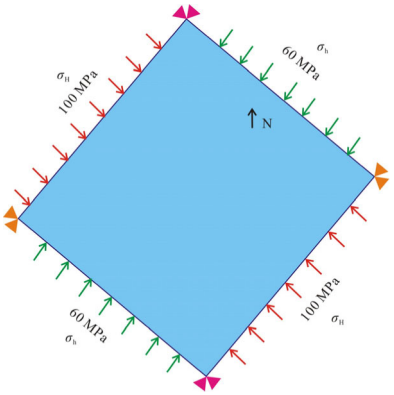

FIGURE 7. Stress loading scheme of the target layer.

C. LOADING SCHEME

According to the research of the previous, the fractures developed in the He8 member tight sandstone were believed to have formed under the strongest period of compressive stress in the Yanshanian period [18], [62]–[64]. The horizontal maximum principal stress was approximately 100 MPa, and the direction was N45°W. Meanwhile. The horizontal minimum principal stress is 0.6 times of the horizontal maximum principal stress [1], [61], [62], [64], [65]. Therefore, the stress loading scheme in this paper is shown in Fig. 7, applying the horizontal compressive stress of 100 MPa and 60 MPa in the N45°W and N45°E directions, respectively. The ratio between the applied maximum and the minimum horizontal stress is 1.67. The vertical stress is achieved by applying a gravitational acceleration [38].

D. PALEO-TECTONIC STRESS FIELD DISTRIBUTION

The planar distributions of each principal stress in the main production layer of the Lower He8 member, shown in Fig. 8a_1 - a_3, are the maximum horizontal stress, minimum horizontal stress and vertical stress of the Lower He8-1 member, respectively, while Fig. 8b_1 - b_3 are the maximum horizontal stress, minimum horizontal stress and vertical stress of the Lower He8-2 member, respectively. The planar distribution characteristics of each principal stress are similar, and the stress shows a strip distribution feature on the plane. The maximum horizontal stress is mainly distributed at 90-125 MPa, the minimum horizontal stress is mainly distributed at 60-90 MPa, and the vertical stress is mainly distributed at 60-64 MPa. The distribution of horizontal stress is mainly affected by lithology and local structure, and the vertical stress is mainly affected by the burial depth. Stress diffusion occurs in some areas, which are mainly affected by lithologic mutations or complex structures.

IV. SWEET SPOT PREDICTION

A. STRAIN ENERGY DENSITY DISTRIBUTION

Strain energy density (U) was used to characterize the distribution of strain within rocks [47], [66]. The presence of microfractures will significantly affect the distribution of strain energy within the rock [67]. Rocks located in areas with high values of strain energy density are more prone to produce ruptures. Therefore, this parameter can be used to determine the probability of internal ruptures in rocks [68]–[70].

Jaeger and Cook [47] provided a detailed description of the derivation of strain energy density. First, consider applying a uniaxial force σ_1 in a quasi-static manner on a cubic rock with a side length a. Then the applied force is $k\sigma_1$, where k is a scalar from 0 to 1. The area of force is a^2 and the force is $k\sigma_1 a^2$. Assuming that the total displacement occurring in the force direction is $a\varepsilon_1$, then the displacement is $ak\varepsilon_1$ at any moment. The incremental work done by this force when k increases from k to $k + \mathrm{d}k$ is [47]

$$\mathrm{d}W = \text{force} \times \text{displacement} = (k\sigma_1 a^2)(a\varepsilon_1 \mathrm{d}k) = \sigma_1 \varepsilon_1 a^3 k \mathrm{d}k \tag{3}$$

The total work of the force is

$$W = \int \mathrm{d}W = \sigma_1 \varepsilon_1 a^3 \int_0^1 k \mathrm{d}k = \frac{1}{2}\sigma_1 \varepsilon_1 a^3 \tag{4}$$

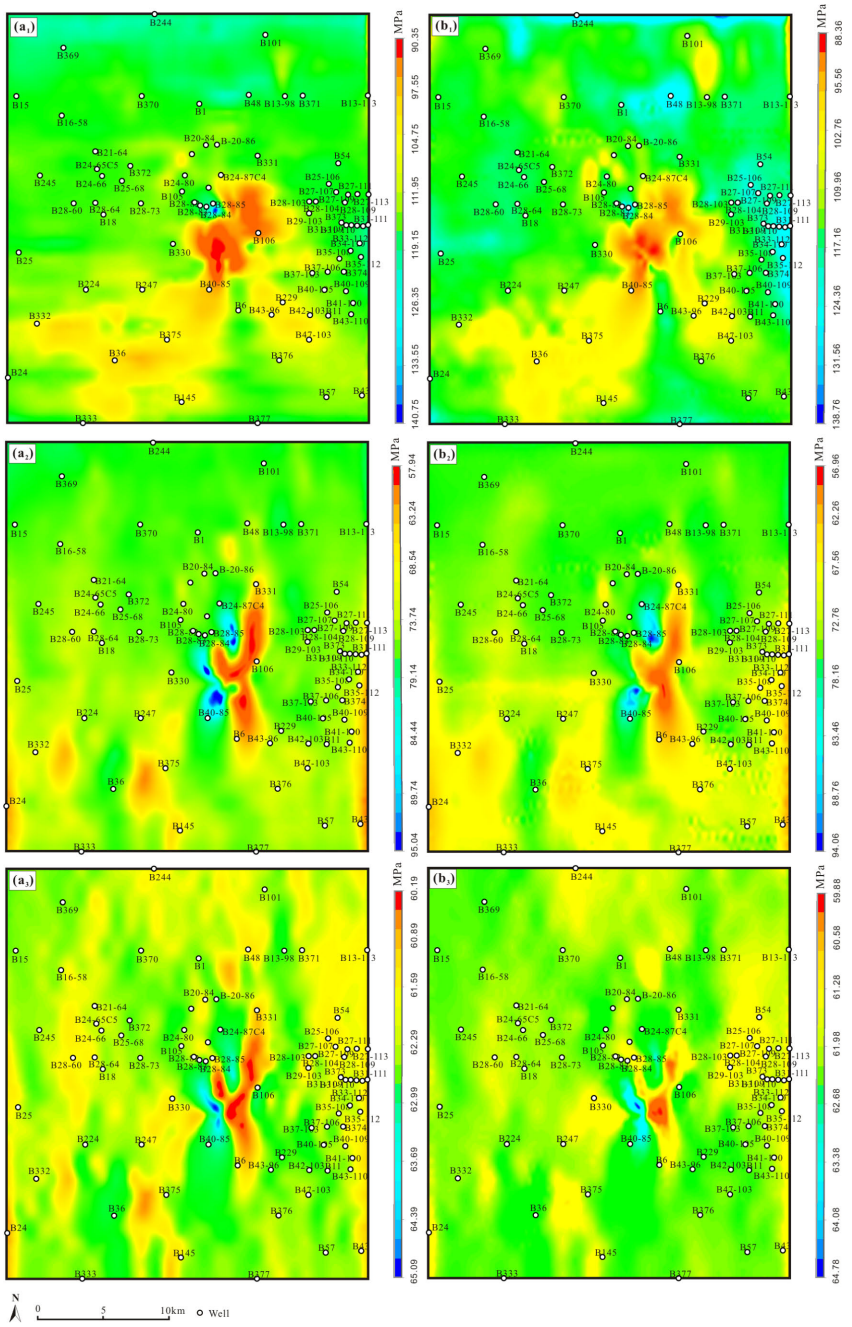

FIGURE 8. Planar distribution of the principal stresses of the target layer. Notes: a_1 - a_3 are the maximum horizontal stress, minimum horizontal stress and vertical stress of the Lower He8-1 member, respectively; and b_1 - b_3 are the maximum horizontal stress, minimum horizontal stress and vertical stress of the Lower He8-2 member, respectively.

The total strain energy (U_{TOT}) is stored in the rock mass and can be expressed as

$$U_{TOT} = \frac{1}{2}\sigma_1\varepsilon_1 a^3 \tag{5}$$

Therefore, the strain energy density (U) can be expressed as

$$U = \frac{U_{TOT}}{a^3} = \frac{1}{2}\sigma_1\varepsilon_1 \tag{6}$$

For triaxial stresses, the total strain energy density can be superimposed [71]. Therefore, the strain energy density of a unit volume inside the rock can be expressed as

$$U = \frac{1}{2}(\sigma_1\varepsilon_1 + \sigma_2\varepsilon_2 + \sigma_3\varepsilon_3) \tag{7}$$

where σ_1, σ_2 and σ_3 are the three principal stresses of the rock in orthogonal coordinates, and ε_1, ε_2 and ε_3 are the three strains of the rock in orthogonal coordinates. The parameter

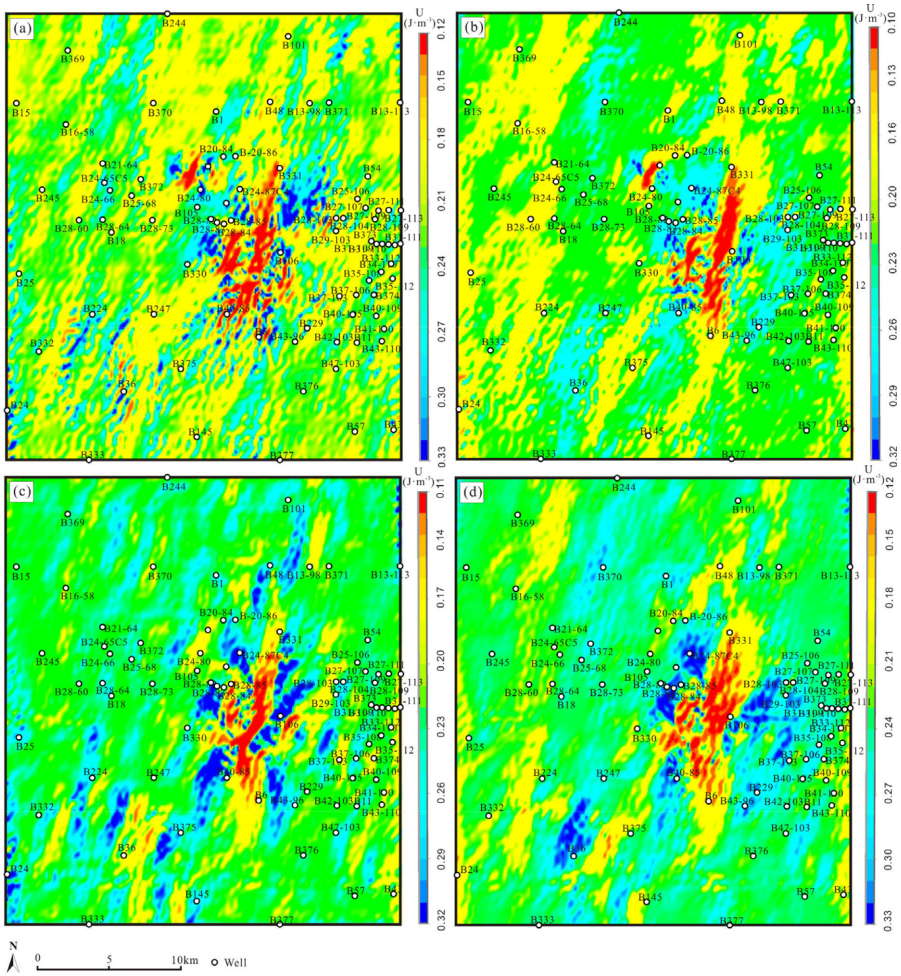

FIGURE 9. Planar distribution of U of the target layer. Notes: (a)-(d) are the Upper He8-1, Upper He8-2, Lower He8-1 and Lower He8-2 members, respectively.

U can also be calculated by the rock mechanics parameter (Young's modulus and Poisson's ratio) and each principal stress [47]:

$$U = \frac{1}{2E}\left[(\sigma_1^2+\sigma_2^2+\sigma_3^2) - 2\upsilon(\sigma_1\sigma_2+\sigma_2\sigma_3+\sigma_3\sigma_1)\right] \quad (8)$$

Based on the paleo-tectonic stress field recovery and the assignment results of rock mechanics parameters, the U distribution of the target layer was determined using Eq. (8). The results are shown in Fig. 9. The U value of the Upper He8 member (Fig. 9a-b) is obviously lower than the Lower He8 member (Fig. 9c-d). This is mainly due to the high mud content of the Upper He8 member. The muddy components have a strong plasticity and are therefore less likely to break [48].

The U values have obvious banded distribution characteristics, and the U values of each layer are mainly distributed between 0.12 and 0.30 J·m^{-3}. The regions with higher U values are mainly distributed in the central and eastern regions of the study area, and their U values are generally greater than 0.24 J·m^{-3} (Fig. 9). A large amount of strain energy accumulates in the rocks with a high U value, and these rocks are prone to have stress concentration and ruptures.

B. RELATIONSHIP BETWEEN STRAIN ENERGY DENSITY AND SINGLE WELL PRODUCTIVITY

Based on the strain energy density calculation of each production layer, the relationship between strain energy density and single well productivity was compared. The production wells were divided into Type I, Type II and Type III wells. The average daily gas production per well of the Type III wells is less than 0.5×10^4 m^3, and its cumulative production is generally less than $1\,000 \times 10^4$ m^3. Such gas wells cannot obtain commercial production capacity. Drilling such gas wells will cause serious manpower and material waste [72], [73]. From the development status of the He8 reservoir in the entire western Sulige gas field, the number of such gas wells is very large, reaching almost 50%. The average daily gas production per well of the Type II wells is between 0.5 and 1×10^4 m^3, and its cumulative production is generally between $1\,000$ and $3\,000 \times 10^4$ m^3. The average daily gas production per well of the Type I wells is greater than

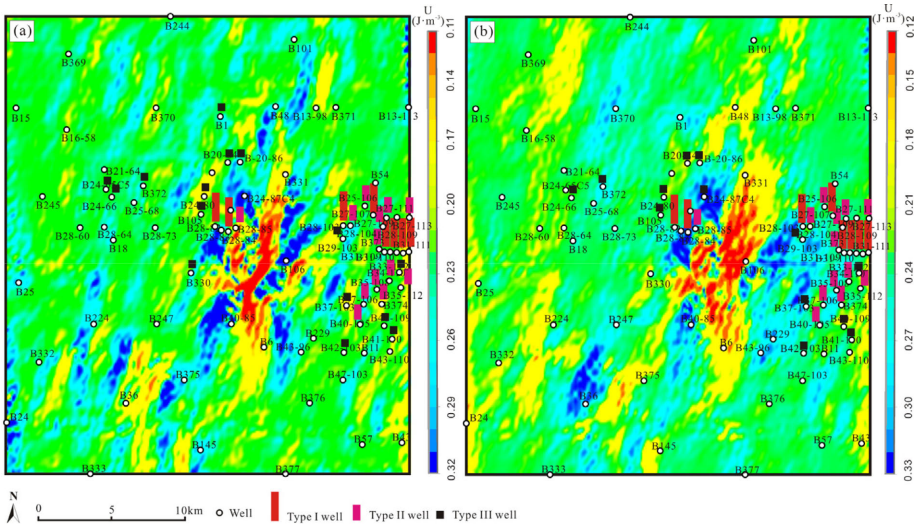

FIGURE 10. Distribution of U value and different types of wells. Notes: (a)-(b) are the Lower He8-1and He8-2 members, respectively.

1×10^4 m^3, and its cumulative production is usually greater than $3\,000 \times 10^4$ m^3. Both the Type I and Type II wells have a good commercial development value.

At present, the production wells in the study area are mainly located in the central and eastern regions, while other areas are mainly exploration wells (Fig. 10). Type I and Type II wells are mainly distributed in the eastern region, while the distribution of the Type III wells is rather scattered. Overall, the Type I and Type II wells are mainly distributed in high U value regions, while the Type III wells are mainly distributed in low U value regions.

To better compare the relationship between single well productivity and U values, the criteria for distinguishing different types of wells based on U values were proposed. When the U value is greater than 0.25 J·m^{-3}, the production well is identified as a Type I well, when the U value is between 0.24 and 0.25 J·m^{-3}, the production well is identified as a Type II well, and when the U value is less than 0.24 J·m^{-3}, the production well is identified as a Type III well. According to this criteria, statistics were conducted on the conformity of different types of wells, which is shown in Table 3. The coincidence rate of the Type I, Type II and Type III wells are 62.5%, 84.6% and 73.3%, respectively. The overall coincidence rate for all wells is 75.0%. For the tight He8 tight sandstone reservoirs in the study area, this coincidence rate can greatly improve the drilling success rate and avoid drilling risks.

C. SWEET SPOT PREDICTION

The sweet spots based on the U value calculations in the Lower He8 member was predicted. The calculated U value is the average value of the Lower He8-1 and He8-2 members. Since the Type I wells and Type II wells both have good commercial development value, according to the criteria shown in Table 3, the area with $U \geq 0.24$ J·m^{-3} was defined as the sweet spot. The distribution of the sweet spots in the Lower He8 member is shown in Fig. 11.

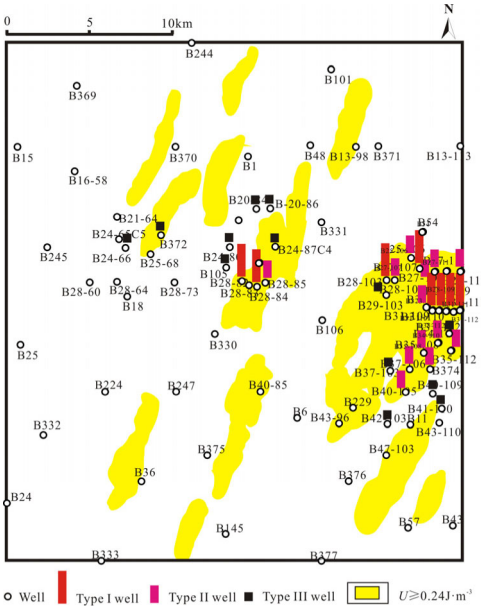

FIGURE 11. Prediction of sweet spot distribution in the Lower He8 member.

As seen from Fig. 11, Type I and Type II wells are distributed in the sweet spot areas, while the Type III wells are generally distributed outside the sweet spot areas.

The sweet spots, defined in this paper according to U-value calculations, are mainly based on rock deformation, stress concentration and micro-scale rupture probability. Micro-fractures are important drainage media for natural gas migration. However, the geological factors affecting the gas-bearing properties of tight sandstones also include such as reservoir properties and preservation conditions.

TABLE 3. Criteria for distinguishing different types of wells based on *U* values.

Well type	*U* value ($J \cdot m^{-3}$)	Total well number	Wells meeting the standard	Coincidence rate (%)	Total coincidence rate (%)
Type I well	$U>0.25$	8	5	62.5	
Type II well	$0.24 \leq U \leq 0.25$	13	11	84.6	75.0
Type III well	$U<0.24$	15	11	73.3	

Therefore, for the sweet spot prediction in the He8 tight sandstone reservoir, the geological factors and *U*-value distributions should both be well considered.

In this paper, a systematic sweet spot forecasting method based on *U* value calculation was proposed. This method is applicable to the strong heterogeneous tight sandstone reservoirs in the low-amplitude tectonic zone of the Ordos Basin and has reference value for similar types of reservoirs around the world.

V. CONCLUSION

(1) In this paper, a systematic forecasting method for sweet spots in a low-amplitude tectonic zone based on *U*-value calculations was proposed.

(2) A new rock mechanics parameter assignment method based on sedimentary facies control principle was proposed. The distribution of horizontal stress is mainly affected by lithology and local structure, and the vertical stress is mainly affected by the burial depth.

(3) The planar distribution of *U* values is characterized by a band-like distribution. The criteria for distinguishing sweet spot areas based on *U* values were proposed, the total coincidence rate is 75.0%.

REFERENCES

[1] W. Ding, P. Dai, D. Zhu, Y. Zhang, J. He, A. Li, and R. Wang, "Fractures in continental shale reservoirs: A case study of the Upper Triassic strata in the SE Ordos Basin, Central China," *Geological Mag.*, vol. 153, no. 4, pp. 663–680, 2016.

[2] J. Lai, G. Wang, Y. Ran, Z. Zhou, and Y. Cui, "Impact of diagenesis on the reservoir quality of tight oil sandstones: The case of Upper Triassic Yanchang Formation Chang 7 oil layers in Ordos Basin, China," *J. Pet. Sci. Eng.*, vol. 145, pp. 54–65, Mar. 2016.

[3] C. Han, M. Han, Z. Jiang, Z. Han, H. Li, Z. Song, W. Zhong, K. Liu, and C. Wang, "Source analysis of quartz from the Upper Ordovician and Lower Silurian black shale and its effects on shale gas reservoir in the Southern Sichuan Basin and its periphery, China," *Geological J.*, vol. 54, no. 1, pp. 439–449, 2019.

[4] D. Lv, D. Wang, Z. Li, H. Liu, and Y. Li, "Depositional environment, sequence stratigraphy and sedimentary mineralization mechanism in the coal bed- and oil shale-bearing succession: A case from the Paleogene Huangxian Basin of China," *J. Petroleum Sci. Eng.*, vol. 148, pp. 32–51, Jan. 2017.

[5] Y.-M. Pang, X.-W. Guo, Z.-Z. Han, X.-H. Zhang, X.-Q. Zhu, F.-H. Hou, C. Han, Z.-G. Song, and G.-L. Xiao, "Mesozoic–Cenozoic denudation and thermal history in the Central Uplift of the South Yellow Sea basin and the implications for hydrocarbon systems: Constraints from the CSDP-2 borehole," *Mar. Petroleum Geol.*, vol. 99, pp. 355–369, Jan. 2019.

[6] T. F. Wan, *Intraplate Deformation and its Uses in the Eastern China*. Beijing, China: Geological Publishing House, (in Chinese), 1993, pp. 79–84.

[7] C. Zou, Z. Yang, G. Zhang, L. Hou, R. Zhu, S. Tao, X. Yuan, D. Dong, Q. Wang, L. Wang, H. Bi, D. Li, and N. Wu, "Conventional and unconventional petroleum 'orderly accumulation': Concept and practical significance," *Petroleum Explor. Develop.*, vol. 41, no. 1, pp. 14–30, 2014.

[8] Y.-T. Cao, L. Liu, C. Wang, L. Kang, D. Li, W.-Q. Yang, and X.-H. Zhu, "Timing and nature of the partial melting processes during the exhumation of the garnet–bearing biotite gneiss in the southern Altyn Tagh HP/UHP belt, Western China," *J. Asian Earth Sci.*, vol. 170, pp. 274–293, Feb. 2019.

[9] Q. Du, Z. Han, X. Shen, C. Han, Z. Song, L. Gao, M. Han, and W. Zhong, "Geochronology and geochemistry of Permo-Triassic sandstones in eastern Jilin Province (NE China): Implications for final closure of the Paleo-Asian Ocean," *Geosci. Frontiers*, vol. 10, pp. 685–704, Mar. 2019. doi: 10.1016/j.gsf.2018.03.014.

[10] W. Ju and K. Wang, "A preliminary study of the present-day in-situ stress state in the Ahe tight gas reservoir, Dibei Gasfield, Kuqa Depression," *Marine Petroleum Geol.*, vol. 96, pp. 154–165, 2018.

[11] H. C. Lau, H. Li, and S. Huang, "Challenges and opportunities of coalbed methane development in China," *Energy Fuels*, vol. 31, pp. 4588–4602, Apr. 2017.

[12] J. Zhao, D. Tang, H. Xu, Y. Lv, and S. Tao, "High production indexes and the key factors in coalbed methane production: A case in the Hancheng block, southeastern Ordos Basin, China," *J. Petroleum Sci. Eng.*, vol. 130, pp. 55–67, Jun. 2015.

[13] C. Zou, R. Zhu, K. Liu, L. Su, B. Bai, X. Zhang, X. Yuan, and J. Wang, "Tight gas sandstone reservoirs in China: Characteristics and recognition criteria," *J. Petroleum Sci. Eng.*, volS. 88–89, pp. 82–91, Jun. 2012.

[14] J. Z. Zhao, J. Li, Q. Cao, Y. B. Bai, C. Er, X. M. Wang, H. Xiao, and W. T. Wu, "Hydrocarbon accumulation patterns of large tight oil and gas fields," (in Chinese with English abstract), *Oil Gas Geol.*, vol. 34, no. 5, pp. 573–583, 2013.

[15] B. D. Cao, "Controlling factors of gas accumulation in the Yuxi gas field in western Shanxi fold belt in Ordos Basin (in Chinese with English abstract)," M.S. thesis, Dept. School Earth Sci. Resour., Chang'an Univ., Xi'an, China, 2012, pp. 61–66.

[16] J. H. Cheng, R. X. Li, X. Qin, D. Li, and B. Zhao, "Impact of diagenetic facies on mechanical properties of sandstone rock in low-permeability reservoirs: A case study of the Upper Paleozoic gas reservoir in east Ordos Basin," (in Chinese with English abstract), *Acta Petrolei Sinica*, vol. 37, no. 10, pp. 1256–1262, 2016.

[17] L.-L. Xiao, J.-C. Wei, C. Niu, L.-Q. Shi, P.-H. Zhai, H.-Y. Yin, and D.-L. Xie, "Study on the distortion of apparent resistivity curves caused by the 'infinite' electrode space of a Pole–Pole array and its correction," *J. Appl. Geophys.*, vol. 118, pp. 124–138, Jul. 2015.

[18] X. H. Liu, Y. M. Feng, J. L. Luo, and T. Lin, "Characteristics of fluid inclusions in reservoirs in the eighth member of the Shihezi Formation and the first member of the Shanxi Formation in Uxin Ju area, the Ordos Basin and their significance," (in Chinese with English abstract), *Oil Gas Geol.*, vol. 31, no. 3, pp. 360–366, 2010.

[19] W. H. Wang, "Research on fluvial sand deposition and heterogeneity to H8 in the east region adjacent to Sulige gas field," Ph.D. dissertation, Dept. School Energy, Chengdu Univ. Technol., Chengdu, China, (in Chinese with English abstract), 2016, pp. 90–100.

[20] Y. Cho, R. L. Gibson, Jr., J. Lee, and C. Shin, "Linear-slip discrete fracture network model and multiscale seismic wave simulation," *J. Appl. Geophys.*, vol. 164, pp. 140–152, May 2019.

[21] J. Lai, G. Wang, Z. Fan, Z. Wang, J. Chen, Z. Zhou, S. Wang, and C. Xiao, "Fracture detection in oil-based drilling mud using a combination of borehole image and sonic logs," *Mar. Pet. Geol.*, vol. 84, pp. 195–214, Jun. 2017.

[22] C. Malatesta, L. Federico, L. Crispini, and G. Capponi, "Fluid-controlled deformation in blueschist-facies conditions: Plastic vs brittle behaviour in a brecciated mylonite (Voltri Massif, Western Alps, Italy)," *Geological Mag.*, vol. 155, no. 2, pp. 335–355, 2017.

[23] A. Ghaderi, J. Taheri-Shakib, and M. A. S. Nik, "The distinct element method (DEM) and the extended finite element method (XFEM) application for analysis of interaction between hydraulic and natural fractures," *J. Petroleum Sci. Eng.*, vol. 171, pp. 422–430, Dec. 2018.

[24] X. Chang, Y. Wang, B. Shi, and Y. Xu, "Charging of Carboniferous volcanic reservoirs in the eastern Chepaizi uplift, Junggar Basin (northwestern China) constrained by oil geochemistry and fluid inclusion," *AAPG Bull.*, vol. 103, no. 7, pp. 1625–1652, 2019. doi: 10.1306/12171818041.

[25] B. Shi, X. Chang, W. Yin, Y. Li, and L. Mao, "Quantitative evaluation model for tight sandstone reservoirs based on statistical methods—A case study of the Triassic Chang 8 tight sandstones, Zhenjing area, Ordos Basin, China," *J. Petroleum Sci. Eng.*, vol. 173, pp. 601–616, Feb. 2019.

[26] H. Wang, "An improved dual-porosity model for the electrical analysis of fractured porous media based on the pore scale method," *J. Appl. Geophys.*, vol. 159, pp. 497–505, Dec. 2018.

[27] J. Feng, J. Dai, J. Lu, and X. Li, "Quantitative prediction of 3-D multiple parameters of tectonic fractures in tight sandstone reservoirs based on geomechanical method," *IEEE Access*, vol. 6, pp. 39096–39116, 2018.

[28] Y. Gan and E. M. Chesnokov, "Effects of variations in fluid properties and fracture geometry on dispersion, anisotropy, and reflection in media with planar fractures," *Geophys. Prospecting*, vol. 66, no. 3, pp. 512–529, 2018.

[29] S. Yin, W. L. Ding, Y. X. Sun, X. H. Wang, M. Zhang, and N. J. Zhang, "Shale uniaxial compressive failure properties and the affecting factors of UCS," *Earth Sci. Frontiers*, vol. 23, no. 2, pp. 75–95, 2016.

[30] S. Zhang, S. Yin, F. Wang, and H. Zhao, "Characterization of in situ stress state and joint properties from extended leak-off tests in fractured reservoirs," *Int. J. Geomech.*, vol. 17, no. 3, pp. 312–315, 2017.

[31] L. Zeng, J. Jiang, and Y. Yang, "Fractures in the low porosity and ultra-low permeability glutenite reservoirs: A case study of the late Eocene Hetaoyuan formation in the Anpeng Oilfield, Nanxiang Basin, China," *Mar. Petroleum Geol.*, vol. 27, pp. 1642–1650, Aug. 2010.

[32] E. M. T. Takougang, Y. Bouzidi, and M. Y. Ali, "Characterization of small faults and fractures in a carbonate reservoir using waveform inversion, reverse time migration, and seismic attributes," *J. Appl. Geophys.*, vol. 161, pp. 116–123, Feb. 2019.

[33] J. Lai, G. Wang, Z. Wang, J. Chen, X. Pang, S. Wang, Z. Zhou, Z. He, Z. Qin, and X. Fan, "A review on pore structure characterization in tight sandstones," *Earth-Sci. Rev.*, vol. 177, pp. 436–457, Jun. 2014.

[34] Q. Meng, J. Hooker, and J. Cartwright, "Lithological control on fracture cementation in the Keuper Marl (Triassic), north Somerset, U.K." *Geological Mag.*, vol. 155, no. 8, pp. 1761–1775, 2018. doi: 10.1017/S001675681700070X.

[35] J. C. Ruf, K. A. Rust, and T. Engelder, "Investigating the effect of mechanical discontinuities on joint spacing," *Tectonophysics*, vol. 295, nos. 1–2, pp. 245–257, 1998.

[36] A. Saein and Z. T. Riahi, "Controls on fracture distribution in Cretaceous sedimentary rocks from the Isfahan region, Iran," *Geological Mag.*, vol. 156, no. 6, pp. 1092–1104, 2019. doi: 10.1017/S0016756817000346.

[37] J. Zhao, D. Tang, Y. Qin, H. Xu, Y. Lv, S. Tao, and S. Li, "Evaluation of fracture system for coal marcolithotypes in the Hancheng Block, eastern margin of the Ordos Basin, China," *J. Petroleum Sci. Eng.*, vol. 159, pp. 799–809, Nov. 2017.

[38] S. Yin, A. Li, Q. Jia, W. Ding, and Y. Li, "Numerical simulation of the in situ stress in a high-rank coal reservoir and its effect on coal-bed methane well productivity," *Interpretation*, vol. 6, no. 2, pp. T271–T281, 2018.

[39] S. Yin and W. Ding, "Evaluation indexes of coalbed methane accumulation in the strong deformed strike-slip fault zone considering tectonics and fractures: A 3D geomechanical simulation study," *Geological Mag.*, vol. 155, no. 6, pp. 1052–1068, 2018.

[40] L. Dong, D. Wang, Y. Zhang, and D. Zhou, "Signal enhancement based on complex curvelet transform and complementary ensemble empirical mode decomposition," *J. Appl. Geophys.*, vol. 144, pp. 144–150, Sep. 2017.

[41] J. Lai, G. Wang, S. Wang, J. Cao, M. Li, X. Pang, Z. Zhou, X. Fan, Q. Dai, L. Yang, Z. He, and Z. Qin, "Review of diagenetic facies in tight sandstones: Diagenesis, diagenetic minerals, and prediction via well logs," *Earth-Sci. Rev.*, vol. 185, pp. 234–258, Oct. 2018.

[42] S. Yin, D. Lv, and W. Ding, "New method for assessing microfracture stress sensitivity in tight sandstone reservoirs based on acoustic experiments," *Int. J. Geomech.*, vol. 18, no. 4, pp. 1–16, 2018.

[43] W. Zeng, W. Ding, J. Zhang, Y. Zhang, L. Guo, K. Jiu, and Y. Li, "Fracture development in Paleozoic shale of Chongqing area (South China). Part two: Numerical simulation of tectonic stress field and prediction of fractures distribution," *J. Asian Earth Sci.*, vol. 75, pp. 267–279, Oct. 2013.

[44] H. Xu, S. Busetti, and C. Arson, "Fracture-induced anisotropy of the stress–strain response of shale at multiple scal," *Int. J. Geomech.*, vol. 17, no. 8, pp. 769–773, 2017.

[45] B. Indraratna, C. Kumara, S.-P. Zhu, and S. Sloan, "Mathematical modeling and experimental verification of fluid flow through deformable rough rock joints," *Int. J. Geomech.*, vol. 15, no. 4, pp. 1–10, 2015.

[46] C. Jacquemyn, M. D. Jackson, and G. J. Hampson, "Surface-based geological reservoir modelling using grid-free NURBS curves and surfaces," *Math. Geosci.*, vol. 51, pp. 1–28, Jan. 2019.

[47] J. C. Jaeger and N. G. W. Cook, *Fundamentals of Rock Mechanics*. London, U.K.: Chapman and Hall, 1976, p. 585.

[48] S. Yin, J. Zhao, Z. Wu, and W. Ding, "Strain energy density distribution of a tight gas sandstone reservoir in a low-amplitude tectonic zone and its effect on gas well productivity: A 3D FEM study," *J. Petroleum Sci. Eng.*, vol. 170, pp. 89–104, Nov. 2018.

[49] X. M. Wang, J. Z. Zhao, X. S. Liu, and L. Y. Fan, "Distribution of formation water in tight sandstone reservoirs of western Sulige gas field, Ordos Basin," (in Chinese with English abstract), *Oil Gas Geol.*, vol. 33, no. 5, pp. 802–810, 2012.

[50] S. Yin, D. Lv, Z. Wu, and W. Ding, "Assemblage of strike-slip faults and tectonic extension and compression analysis: A case study of a Lower Permian commercial coal reservoir in China," *J. Earth Syst. Sci.*, vol. 127, pp. 1–15, Aug. 2018.

[51] S. L. Xi, W. H. Li, X. S. Wei, P. L. Meng, and J. P. Feng, "Study on the characteristics of quartz sandstone reservoir of the Neopaleozoic of two gasfields in Ordos Basin," (in Chinese with English abstract), *Acta Sedimentologica Sinica.*, vol. 27, no. 2, pp. 221–229, 2009.

[52] C. Ma, T. Li, H. Zhang, Y. Jiang, and T. Song, "A method for numerical simulation based on microseismic information and the interpretation of hard rock fracture," *J. Appl. Geophys.*, vol. 164, pp. 214–224, May 2019.

[53] S. Yin, R. Xie, Z. Wu, J. Liu, and W. Ding, "In situ stress heterogeneity in a highly developed strike-slip fault zone and its effect on the distribution of tight gases: A 3D finite element simulation study," *Mar. Petroleum Geol.*, vol. 99, no. 1, pp. 75–91, 2019.

[54] S. Salimzadeh and N. Khalili, "Fully coupled XFEM model for flow and deformation in fractured porous media with explicit fracture flow," *Int. J. Geomech.*, vol. 16, no. 4, pp. 434–438, 2016.

[55] E. L. Olson and M. L. Cooke, "Application of three fault growth criteria to the Puente Hills thrust system, Los Angeles, California, USA," *J. Struct. Geol.*, vol. 27, pp. 1765–1777, Oct. 1993.

[56] B. A. Camac and S. P. Hunt, "Predicting the regional distribution of fracture networks using the distinct element numerical method," *AAPG Bull.*, vol. 93, no. 11, pp. 1571–1583, 2009.

[57] Y. Eyal, M. R. Gross, T. Engelder, and A. Becker, "Joint development during fluctuation of the regional stress field in southern Israel," *J. Struct. Geol.*, vol. 23, nos. 2–3, pp. 279–296, 2001.

[58] J. Zhang, H. Deng, J. Deng, and B. Ke, "Development of energy-based brittleness index for sandstone subjected to freeze-thaw cycles and impact loads," *IEEE Access*, vol. 6, pp. 48522–48530, 2018.

[59] M. R. Gross, M. P. Fischer, T. Engelder, and R. J. Greenfield, "Factors controlling joint spacing in interbedded sedimentary rocks: Integrating numerical models with field observations from the Monterey Formation, USA," in *Fractography: Fracture Topography as a Tool in Fracture Mechanics and Stress Analysis*, vol. 92, M. S. Ameen, Ed. Geological Society, London, U.K.: Special Publications, 1995, pp. 215–233.

[60] R. Gui and Y. P. Wan, "Rock mechanics parameters calculation based on conventional logging data: A case study of upper Paleozoic in Ordos basin," *J. Geomech.*, (in Chinese with English abstract), vol. 18, no. 4, pp. 418–424, 2012.

[61] D. W. Zhu, "Developmental characteristics, major regulating factors and distribution prediction of fractures in shale of upper triassic Yangchang formation in Yangchang oil-gas field," M.S. thesis, China Univ. Geosci., Beijing, China, (in Chinese with English abstract), 2013, pp. 44–54.

[62] J. B. Li, X. N. Wu, Z. J. Zhao, and F. P. Li, "Characteristics and original of Upper Paleozoic fractures in Sulige gas field," (in Chinese with English abstract), *J. Xi'an Univ. Sci. Technol.*, vol. 36, no. 3, pp. 414–419, 2016.

[63] Y. P. Wan, Y. Y. Li, and X. Liang, "Fractures of reservoirs inferred from fluid inclusions: A case study on the upper paleozoic of northern Shaanxi slope," (in Chinese with English abstract), *Geol. Explor.*, vol. 46, no. 4, pp. 711–715, 2010.

[64] W. Zhou, S. N. Zhang, L. Li, and F. Y. Su, "The character of Upper Paleozoic reservoir fractures and the evaluation of their distribution in Tabamiao," (in Chinese with English abstract), *J. Mineral Petroleum*, vol. 26, no. 4, pp. 54–61, 2006.

[65] Y. P. Wan, H. L. Li, Y. Li, Z. J. Song, Y. Y. Li, and P. W. Qi, "The field stress between Late Jurassic and Early Cretaceous in the Eastern Ordos Basin," (in Chinese with English abstract), *Earth Sci.*, vol. 42, no. 4, pp. 499–556, 2017.

[66] Z. Ye, Q. Jiang, C. Zhou, and Y. Liu, "Numerical analysis of unsaturated seepage flow in two-dimensional fracture networks," *Int. J. Geomech.*, vol. 17, no. 5, pp. 543–547, 2017.
[67] V. Demyanov, D. Arnold, T. Rojas, and M. Christie, "Uncertainty quantification in reservoir prediction: Part 2—Handling uncertainty in the geological scenario," *Math. Geosci.*, vol. 51, no. 2, pp. 241–264, 2018.
[68] H. Chen, G. Zhang, T. Chen, and X. Yin, "Joint PP-and PSV-wave amplitudes versus offset and azimuth inversion for fracture compliances in horizontal transversely isotropic media," *Geophys. Prospecting*, vol. 66, no. 3, pp. 561–578, 2018.
[69] Y. Du and A. Aydin, "The maximum distortional strain energy density criterion for shear fracture propagation With applications to the growth paths of *En Échelon* faults," *Geophys. Res. Lett.*, vol. 20, pp. 1091–1094, Jun. 1993.
[70] A. Ghaderi, J. Taheri-Shakib, and M. A. Sharifnik, "The effect of natural fracture on the fluid leak-off in hydraulic fracturing treatment," *Petroleum*, vol. 5, no. 1, pp. 85–89, 2019.
[71] M. D. G. Salamon, "Energy considerations in rock mechanics: Fundamental results," *J. Southern Afr. Inst. Mining Metall.*, vol. 84, pp. 233–246, Aug. 1984.
[72] S. Yin, T. Tian, and Z. Wu, "Developmental characteristics and distribution law of fractures in a tight sandstone reservoir in a low-amplitude tectonic zone, eastern Ordos Basin, China," *Geological J.*, vol. 54, no. 6, p. 115, 2019.
[73] J. Liu, W. Ding, R. Wang, S. Yin, H. Yang, and Y. Gu, "Simulation of paleotectonic stress fields and quantitative prediction of multi-period fractures in shale reservoirs: A case study of the Niutitang Formation in the Lower Cambrian in the Cen'gong block, South China," *Mar. Petroleum Geol.*, vol. 84, pp. 289–310, Jun. 2017.

SHUAI YIN received the B.Sc. degree in geological engineering from the Shandong University of Science and Technology, China, the M.Sc. degree in oil and gas field development geology from the Chengdu University of Technology, China, and the Ph.D. degree in mineral survey and exploration from the China University of Geosciences, Beijing. He is currently a Lecturer with Xi'an Shiyou University. His research interests include physical simulation and fracture prediction in tight oil and gas fields.

ZHIYOU GAO received the B.Sc. degree from the Shandong University of Science and Technology, China, and the M.Sc. degree from the China University of Geosciences, Beijing, both in geological engineering. He is currently a Senior Engineer with Shandong Geo-Mineral Engineering Group, China. His research interest includes geological prospecting.